Metal-directed thiophene-carboxylate-based nickel(II) complexes as multifunctional electrochemical and fluorescent sensors for detecting different analytes

Xiangxiang Liu[1] · Yajun Mu[1] · Jing Zhao[1] · Zhong Zhang[1] · Pengpeng Shao[2] · Guocheng Liu[1,2] · Xiaohui Li[1] · Yongqiang Chen[3]

Abstract

To investigate the effect of the sites of S-atoms in thiophene carboxylates on the structures of coordination polymers, two thiophene-mono-carboxylic acids (2-Htpc = thiophene-2-carboxylic acid and 3-Htpc = thiophene-3-carboxylic acid) and a fluorescent active semi-rigid amide [N,N′-bis(3-methyl pyridine-3-yl)-2,6-naphthalenediamide (L)] were selected to combine with electrochemically active metal ions of Ni(II), and two new coordination polymers (CPs), namely $[Ni_{0.5}(L)_{0.5}(2\text{-tpc})]$ $(H_2O)]\bullet1.5H_2O$ (1) and $[Ni_{0.5}(L)_{0.5}(3\text{-tpc})](H_2O)]\bullet1.5H_2O$ (2), were obtained through traditional hydrothermal methods. The single-crystal X-ray diffraction analyses of the two CPs show that there are similar zigzag chains with the crossed-stacking modes. The two CPs can act as multifunctional electrochemical sensors to detect NO_2^-, chloramphenicol, and L-ascorbic acid (AA) and fluorescent recognition of Fe^{3+} and $Cr_2O_7^{2-}$. The detection limits of 1 were 1.08×10^{-6}, 1.18×10^{-4}, and 1.06×10^{-4} for AA, Fe^{3+}, and $Cr_2O_7^{2-}$. The corresponding values of 2 were 1.43×10^{-6}, 2.06×10^{-4}, and 2.06×10^{-4}.

Xiangxiang Liu and Yajun Mu have contributed equally to this work.

✉ Guocheng Liu
lgch1004@sina.com

✉ Xiaohui Li
lixh@bhu.edu.cn

✉ Yongqiang Chen
chenjzxy@126.com

[1] Professional Technology Innovation Center of Liaoning Province for Conversion Materials of Solar Cell, College of Chemistry and Materials Engineering, Bohai University, Jinzhou 121013, People's Republic of China

[2] Key Laboratory of Cluster Science Ministry of Education, Beijing Key Laboratory of Photoelectronic/Electrophotonic, Advanced Research Institute of Multidisciplinary Science, School of Chemistry and Chemical Engineering, Beijing Institute of Technology, Beijing 100081, People's Republic of China

[3] College of Chemistry and Chemical Engineering, Jinzhong University, Jinzhong 030619, Shanxi, People's Republic of China

Introduction

The rapid development of industry and agriculture has caused different degrees of damage to the environment [1–5]. Although people's awareness of environmental protection has been obviously improved, pollutants such as nitrite (NO_2^-), dichromate ($Cr_2O_7^{2-}$), and antibiotics constantly destroy the balance of the ecosystem [6–10]. The above different pollutants can be successfully detected by different detection methods of spectrophotometry, chromatography, mass spectrometry, etc. [11–16]. However, the simultaneous detection of multiple pollutants is still a great challenge at present [17, 18]. Therefore, it is of great academic significance and application value to develop multifunctional detection materials to realize the simultaneous detection of the above pollutants.

At present, coordination polymer materials are used to realize electrochemical detection and fluorescence sensing detection which are the two effective detection methods [19–23]. Generally speaking, coordination polymer materials based on iron, cobalt, nickel, and copper have good electrochemical detection ability because of their reversible redox activity [24–27]. Coordination polymer materials constructed by organic ligands with appropriate conjugate volume can realize fluorescence detection of pollutants [28,

29]. Therefore, it will be an effective method to construct multifunctional electrochemical and fluorescent detection materials by reasonably utilizing the above two components to construct coordination polymers [30, 31].

Based on the above considerations, Ni^{2+} and [N,N′-bis(3-methylpyridin-3-yl)-2,6-naphthalenediamide (L)] were selected to combine with two thiophene-mono-carboxylic acids (2-Htpc = thiophene-2-carboxylic acid and 3-Htpc = thiophene-3-carboxylic acid). (i) Nitrogen-containing ligands with amide groups are not only stable in structure and strong in space expansion but also have multiple hydrogen bonding sites, which provide opportunities for the formation of supramolecular structures. (ii) Nickel can be coordinated and is electrochemically active. (iii) S-heterocarboxylic acid can be used as O-donating ligand, and its better hydrophilicity is more conducive to the realization of electrocatalytic performance [32–34]. As a result, two one-dimensional (1D) CPs with the crossed-stacking modes, namely $[Ni_{0.5}(L)_{0.5}(2\text{-tpc})](H_2O)]\bullet1.5H_2O$ (1) and $[Ni_{0.5}(L)_{0.5}(3\text{-tpc})](H_2O)]\bullet1.5H_2O$ (2), were obtained and structurally characterized. The good electrochemical sensing properties for KNO_2, chloramphenicol (CAP), and ascorbic acid (AA) were investigated by 1 − 2 modified carbon paste electrode (1–2-CPEs). In addition, the fluorescence sensing properties of the 1 − 2 for Fe^{3+} and $Cr_2O_7^{2-}$ were also studied.

Experimental

Synthetic procedure of 1–2

Preparation of $[Ni_{0.5}(L)_{0.5}(2\text{-tpc})](H_2O)]\bullet1.5H_2O$ (1)

A mixture of $NiCl_2\cdot6H_2O$ (0.0475 g), **L** (0.0393 g), 2-Htpc (0.0321 g), NaOH solution (1.8 mL, 0.1 mol/L), and H_2O (7.5 mL) was sealed in a 25-mL Teflon-lined autoclave and heated at 120 °C for 4 days. The obtained crystals in the autoclave were cooled in the air. After reaching room temperature, light blue crystals of **1** can be collected with a yield of 25% based on L. Calcd for $C_{34}H_{36}N_4NiO_{11}S_2$: C, 51.08; H, 4.54; N, 7.01%. Found: C, 51.10; H, 4.50; N, 7.03%. IR(KBr, cm^{-1}): 3384 m, 3327 m, 3073 m, 2925 m, 1928 w, 1852 w, 1641 s, 1531 s, 1422 s, 1268 s, 1194 m, 928 m, 801 m, 776 s, 714 s, 660 m, 614 w, 537 w.

Preparation of $[Ni_{0.5}(L)_{0.5}(3\text{-tpc})](H_2O)]\bullet1.5H_2O$ (2)

The preparation procedure of complex **2** was similar to that of **1**, but the difference was that 3-Htpc was used instead of 2-Htpc. The obtained crystals in the autoclave were cooled in the air. After reaching room temperature, light blue crystals of **2** can be collected with a yield of 20% based on L. Calcd for $C_{34}H_{36}N_4NiO_{11}S_2$: C, 51.08; H, 4.54; N, 7.01%. Found: C, 51.12; H, 4.46; N, 7.05%. IR (KBr, cm^{-1}): 3371 m, 3324 m, 3100 m, 3069 m, 1929 w, 1855 w, 1639 s, 1530 s, 1416 s, 1264 s, 1191 m, 933 m, 801 m, 769 s, 706 s, 650 m, 624 w, 545 w.

Results and discussion

Description of the crystal structure characteristics of 1–2

$[Ni_{0.5}(L)_{0.5}(2\text{-tpc})](H_2O)]\cdot1.5H_2O$ (1) and $[Ni_{0.5}(L)_{0.5}(3\text{-tpc})](H_2O)]\cdot1.5H_2O$ (2)

To explore the effect of S-sites of thiophene carboxylic acid, 2-tpc (the S-site is in ortho position of the carboxyl group) and 3-tpc (the S-site is in ortho position of the carboxyl group) were selected. However, two isostructural one-dimensional structures of 1 and 2 with subtle structural differences were received. In both structures, Ni atoms and one of the water molecules are located in a special position on a twofold axis. They are both in the monoclinic system with $C2/c$ and contain half Ni^{2+}, half L, one coordinated water molecule, one and a half non-coordinated water molecules, and one tpc anion (2-tpc in 1 and 3-tpc in 2) (Fig. 1a). Each Ni^{2+} has a representative hexacoordination configuration, which is in contact with two pyridine N atoms from two L [Ni − N are 2.106(18) Å in 1 and 2.104(3) Å in 2] and two carboxylic O atoms [Ni − O are 2.048(15) Å in 1 and 2.041(3) Å in 2] and two H_2O [Ni − O are 2.102(14) Å in 1 and 2.097(2) Å in 2] (Table S1 and S2). In 1 and 2, each Ni^{2+} coordinated with two 2-tpc/3-tpc anions and two H_2O to form monometallic subunits $[Ni(L)(2\text{-tpc})_2](H_2O)_2]$ for 1 and $[Ni(L)(3\text{-tpc})_2](H_2O)_2]$ for 2. Each subunit is bridged by adjacent μ_2-L to generate a 1D wave-like chain (Fig. 1b). The above chains were stacked in a crossed manner forming 3D supramolecular frameworks extended by H-bonds (Fig. 1c and d). The details of H-bonds are listed in Table S3 and Fig. S1.

In addition, several subtle differences in the structural details of 1 and 2 were found by deep analysis. The Ni•••Ni distances linked by L are 15.925(8) and 15.854(12) Å. The dihedral angles between pyridine and naphthalene rings are 49.11 and 47.96°. The dihedral angles between the thiophene and pyridine rings are 86.45° and 87.34°, respectively. If the 1D title complexes are considered as one-dimensional chains, the torsion angles of the two crossed CPs are 43.649(1)° and 43.657(1)°. The above structural subtle differences can be attributed to the different S-sites of thiophene carboxylic acid used in the synthesis of the complexes. Although the structures of the title complexes show the above subtle differences, they are not significant. The possible main reason is that the S-atoms of 2-tpc in 1 and 3-tpc in 2 are not coordinated with metal ions. In addition, the corresponding thiophene rings have similar steric hindrance

Fig. 1 a The coordination environment of the Ni^{2+} in **1**; **b** 1D wave-like chain; **c** stacking mode; **d** schematic view of stacking mode
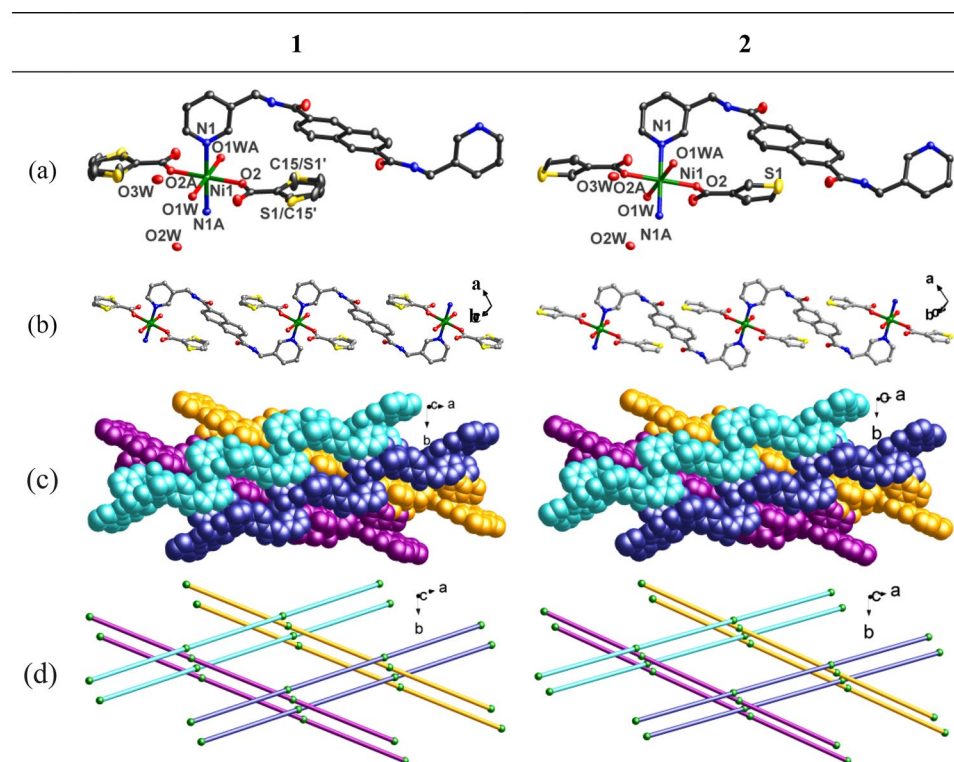
and conjugate volume, which cannot have a significant effect on the coordination of the title complexes. Nickel ion has a typical and relatively fixed hexacoordination mode. Based on the above analyses, the similar 1D wave-type structures of 1 and 2 are directed by center metal ions.

Electrocatalytic activities of the prepared electrodes

With the improvement of people's awareness of environmental protection, water environment has attracted widespread attention [35, 36]. Therefore, a fast, simple, and convenient sensor is needed to detect some analytes in water. Because of its reversible single-electron redox process, CP based on Ni^{2+} is very attractive for electrochemical research [37]. Because 1–2 has the characteristics of water stability and clear composition (Fig. S2), it also has good crystallinity (Fig. S3), successfully fabricated 1–2 bulk modified carbon paste electrodes (n-CPE, n = 1–2) based on the previous literature [38, 39]. Their electrochemical sensing studies were carried out in 0.1 M H$_2$SO$_4$ + 0.5 M Na$_2$SO$_4$ aqueous solution. As can be seen in Fig. S4, the cyclic voltammograms of 1–2-CPE in the same potential range of −200 ∼ +400 mV under different scan rates were displayed. One pair of obvious reversible redox peaks was observed. The oxidation peaks were at 220 mV and 233 mV, and the corresponding reduction peaks of 1–2-CPE were at −19 and −53 mV. With 40 mV s^{-1} as the scan rate, the measured relative mean peak potentials of the pair of peaks [E$_{1/2}$ = (E$_{pa}$ + E$_{pc}$)/2]

were 100.5 mV and 90 mV, respectively, which should be due to the redox between Ni^{III} and Ni^{II} [40, 41]. When the scan rates were increased from 20 mV s^{-1} to 100 mV s^{-1}, the anodic oxidation peak and the corresponding cathodic reduction peak potential moved in the positive and negative directions, respectively. The corresponding peak-to-peak currents of the cathode and anode increased linearly with the increase in the scan rate, and the average peak potential did not change much. This phenomenon expresses that the redox process of 1–2-CPEs was controlled by the surface [42].

The electrocatalytic reduction of KNO$_2$, chloramphenicol (CAP), and oxidation of ascorbic acid (AA) for 1–2-CPEs in the 0.5 M Na$_2$SO$_4$ + 0.1 M H$_2$SO$_4$ aqueous solution was also investigated. As we all know, bare CPE has no obvious response to KNO$_2$, CAP, or AA in an aqueous solution of 0.5 M Na$_2$SO$_4$ + 0.1 M H$_2$SO$_4$ [43]. Figure 2 shows the cyclic voltammograms of the electrocatalytic reduction of KNO$_2$ under 1–2-CPEs. After adding a certain amount of KNO$_2$, it can be seen that all the currents of reduction peak and the corresponding currents of oxidation peak decreased and increased, respectively. It can be concluded that 1–2-CPEs had electrocatalytic reduction ability for NO$_2^-$ [44]. It can be seen from Fig. 3 that the reduction peak current of 1–2-CPEs increased significantly after adding CAP, which can indicate that 1 and 2 had good electrocatalytic activities for the reduction of CAP. In order to study the relationship between concentrations and peak currents, differential pulse voltammetry (DPV) was
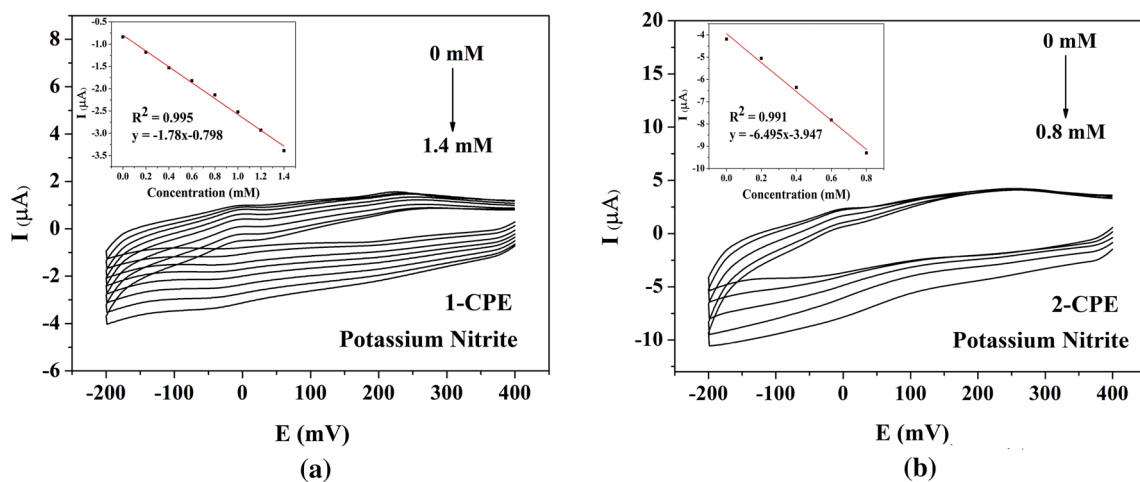
Fig. 2 a-b Cyclic voltammograms plots of **1–2**-CPEs after adding different concentrations of KNO_2 at a sweep speed of 40 mV s^{-1}
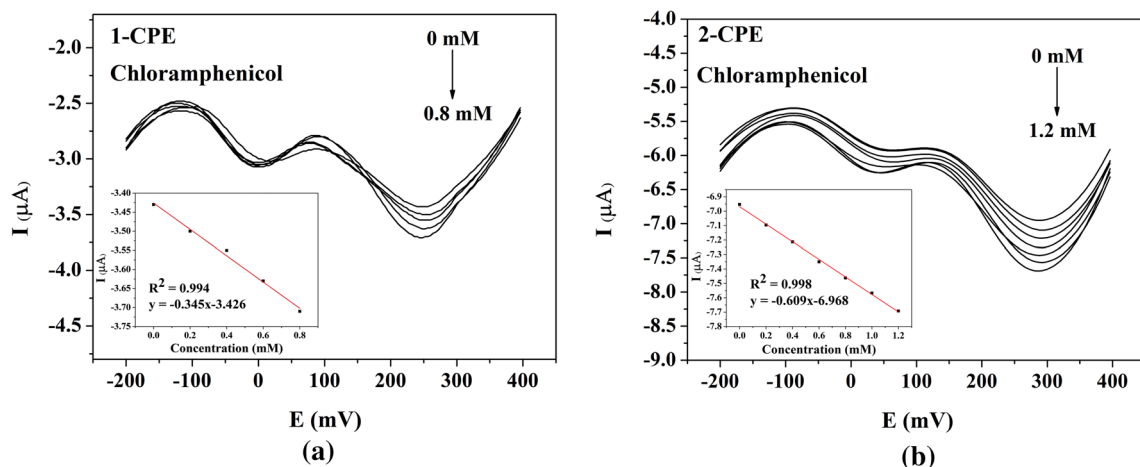

Fig. 3 a-b Differential pulse diagrams of **1–2**-CPEs under different CAP concentrations at a sweep speed of 40 mV s^{-1}

used. With the addition of a certain amount of CAP, the peak currents of 1–2-CPEs increased linearly. This result indicated that 1 and 2 can also be used as effective electrochemical catalysts for CAP [43]. As shown in Fig. 4a and b, after a certain amount of AA was added, the currents of oxidation peak and reduction peak of 1–2-CPEs gradually increased and remained unchanged, respectively, which proved that 1–2-CPEs exhibited excellent electrocatalytic activities for the oxidation of AA [45]. There was a good linear relationship between the peak current intensity and the concentration of AA, which made them be a potential material for AA electrochemical analysis and detection. The above results display that the 1–2-CPEs are multifunctional detection materials with excellent electrocatalytic activities, which can not only reduce KNO_2 and CAP but also oxidize AA. In addition, to evaluate the analytic

performance of 1 and 2 for AA determination quantitatively, the 1–2-CPEs were used as the AA amperometric sensors, respectively [46]. Under continuous stirring, add a certain concentration and volume of AA in 0.5 M $Na_2SO_4 + 0.1$ M H_2SO_4 aqueous solution every 30 s. As shown in Fig. 4c and d, the response time of 1 and 2 was almost 2 s and 1 s, respectively, and it was pointed out that the rapid electroreduction activities of these CPs can prevent the accumulation of reducing intermediates on the electrode surface. In addition, within a certain concentration range, the detection response of 1–2-CPEs to AA was linear. The detection limit of **1–2** was 1.08×10^{-6} and 1.43×10^{-6} (signal-to-noise ratio: 3), respectively. All in all, the **1–2**-CPEs can be used as multifunctional electrochemical sensors, not only can detect KNO_2 and CAP, but also can detect AA, which may expand the application of CPs-based complexes.
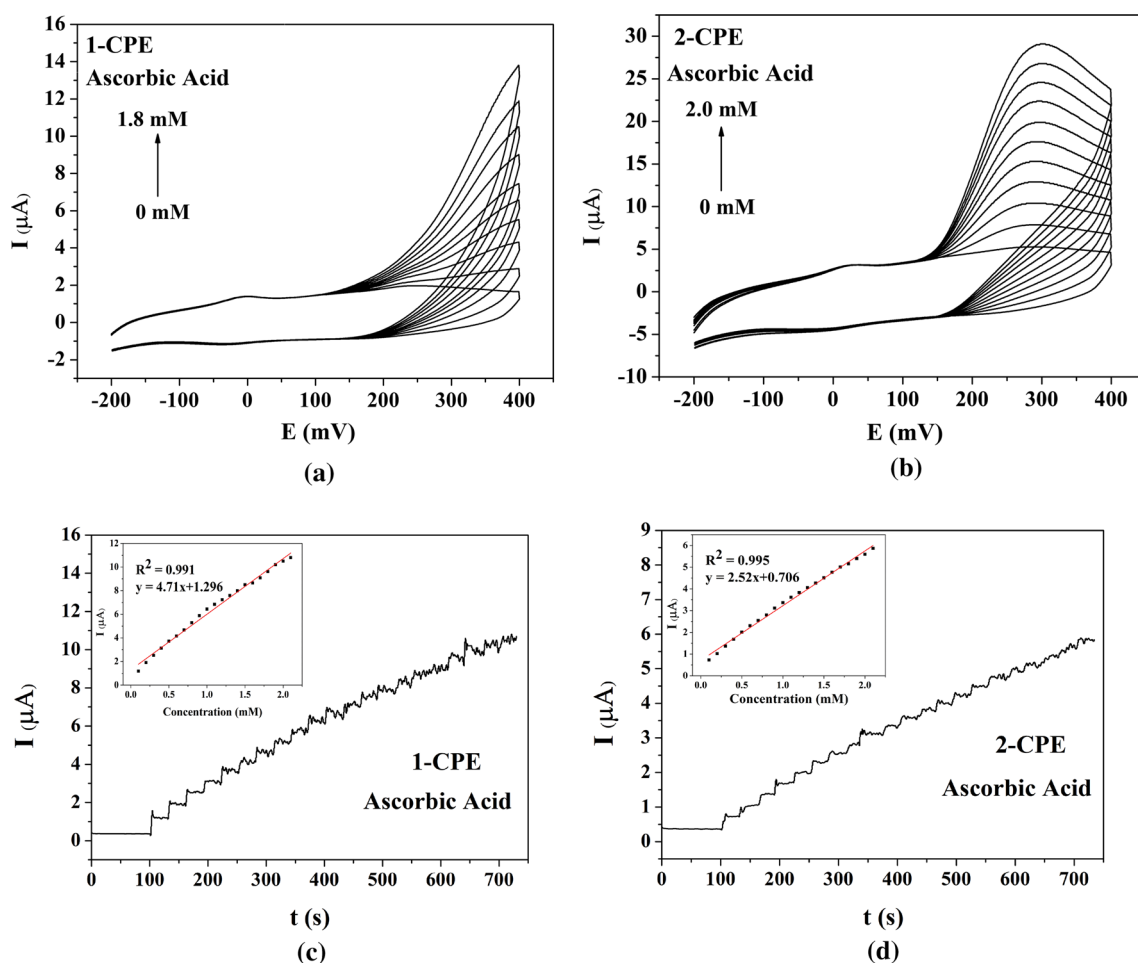
Fig. 4 **a-b** Cyclic voltammograms of **1–2**-CPEs at different AA concentrations at a sweep speed of 40 mV s^{-1}; **c-d** amperometric current responses of **1–2**-CPEs upon addition of AA, respectively. The inset: plots of the concentrations of AA vs the oxidation currents for **1–2**-CPEs, respectively (applied potential: 400 mV for **1**-CPE, 320 mV for **2**-CPE)

Luminescent properties of 1–2

In order to explore the luminescence of 1–2, the solid-state fluorescence properties of 1–2 and the organic L ligand were investigated under the same experimental conditions (slit: 2.5 nm, voltage: 700) at ambient temperature (Fig. S5a). When the excitation at 360 nm was given, it is found that the maximum emission peaks of 1–2 and the L ligand appeared at 379 nm, 380 nm, and 372 nm, respectively. It is well known that there were only weak p* → n transitions, and the carboxylates had very little effect on the photoluminescence of 1–2 [47]. In addition, the solid ultraviolet absorption spectra showed that both the ligand L and the complexes 1–2 had strong absorption peaks in the ultraviolet region of 200–400 nm (Fig. S5b). Thus, the emissions of 1–2 may be assigned to intraligand charge transitions of the organic L ligand [48]. A certain red shift occurred from the L ligand to 1–2, which may be caused by the coordination of organic L ligands to the metal centers [49].

Fluorescence sensing detection of metal cations

Fe^{3+} played an important role in the process of human metabolism. If the human body contained high content of Fe^{3+}, it will cause some cancers and some organ abnormalities [7, 50]. Therefore, it was necessary to adopt a simple method to determine whether Fe^{3+} was contained in the aqueous solution and its content. First, according to the method in the literature, the fluorescence sensing abilities of 1–2 to metal cations were explored [51]. Using 1 as an example, disperse the 3 mg fine powder of 1 as evenly as possible in 3 mL $M(NO_3)_x$ aqueous solution(10^{-2} M) (M is Ba^{2+}, Cd^{2+}, Co^{2+}, Cu^{2+}, K^+, La^{3+}, Na^+, Ni^{2+}, Zn^{2+}, and Fe^{3+}). As shown in Fig. 5a, among the added cations, only Fe^{3+} ion makes the fluorescence quenching effect of 1 remarkable. Fe^{3+} has a similar quenching effect on polymer 2 (Fig. S6a) (Table 1).
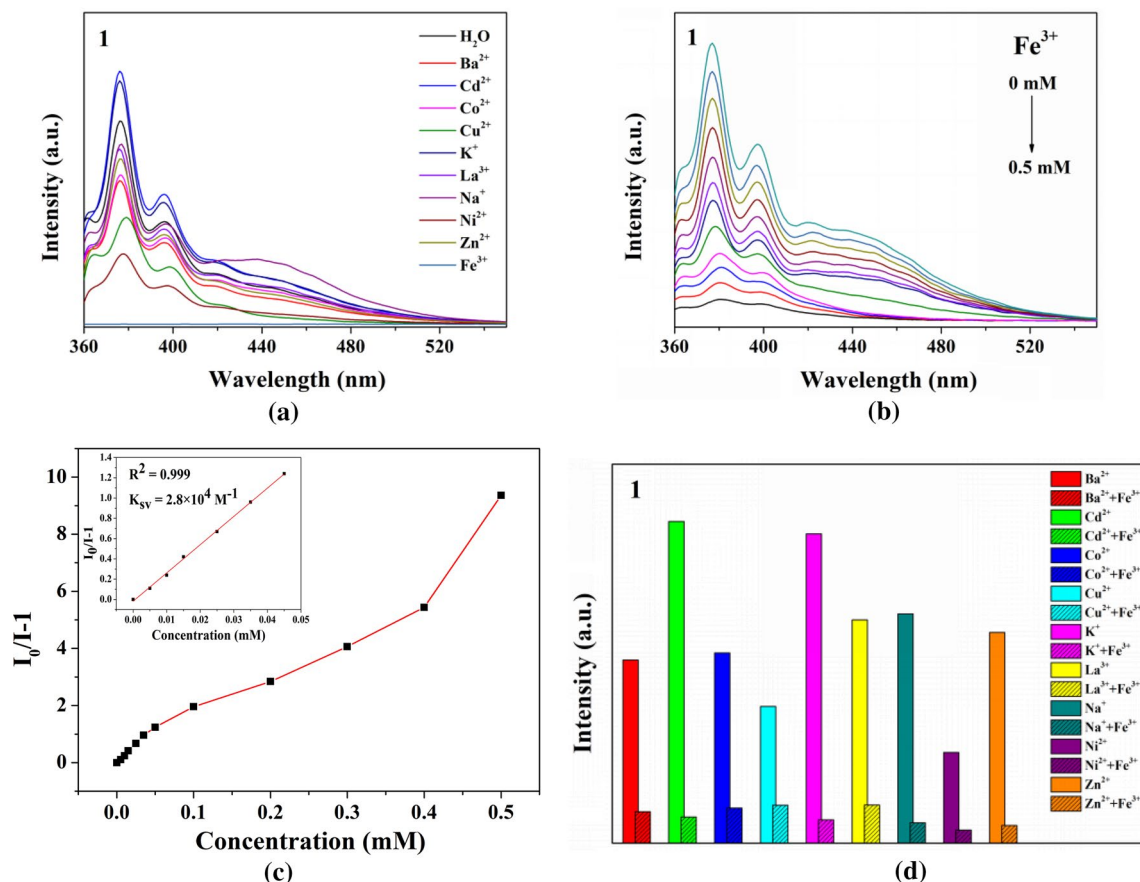
Fig. 5 a Fluorescence emission peak intensity of **1** in different metal cation solutions at the same excitation wavelength. **b** Fe^{3+} (10^{-3} M) concentration gradient experiment. **c** Linear relationship plot between fluorescence intensity and Fe^{3+} ions concentration. **d** Comparison of the luminescence emission peak intensity of **1** upon the addition of Fe^{3+}

To explore the sensitivity of Fe^{3+}, a concentration gradient experiment was carried out by adding an appropriate amount of 10^{-3} M Fe^{3+} solution. As can be seen in Fig. 5b, when the concentration of Fe^{3+} gradually increased, the emission peak intensity of 1 gradually decreased. In addition, the Stern–Volmer constant (K_{SV}, $K_{SV} = [I_0/I - 1]/C$) and the detection limit ($3\sigma/K_{SV}$) of 1 were calculated to be 2.8×10^4 and 1.18×10^{-4}, respectively. It can be seen that polymer 1 showed a better linear relationship at a lower concentration, which may be caused by the static quenching of Fe^{3+}(Fig. 5c) [52]. The concentration gradient of 2 was similar to that of 1, which can indicate that this phenomenon of fluorescence quenching may be caused by the electron transfer between Fe^{3+} and the organic ligand L [48]. It was also necessary to explore the anti-interference effect of 1 in the presence of other metal cations. Fe^{3+} was added to the solution of other cations in 2 at the same time. The result is shown in Fig. 5d. It can be seen that after adding other interfering cations, Fe^{3+} can still

quench 1. Polymer 2 shows the same effect (Fig. S6b–d, and Table 2).

Fluorescence sensing detection of inorganic anions

Some industry wastewater contains a large amount of heavy metal ions such as $Cr_2O_7^{2-}$, so it is very important to detect it quickly [53]. Use the same experimental procedure as cations to measure 10 anions, namely Cl^-, Br^-, I^-, CH_3COO^-, CO_3^{2-}, HCO_3^-, NO_3^-, OH^-, SO_4^{2-}, and $Cr_2O_7^{2-}$. As shown in Fig. 6a, it can be found that $Cr_2O_7^{2-}$ can significantly quench the fluorescence intensity of 1 suspension. Polymer 2 shows similar effects (Fig. S7a). From Fig. 6b and c, it can be found that when the concentration of $Cr_2O_7^{2-}$ ion slowly increased, the luminescence intensity of 1 gradually decreased. From the SV plot, it can be obtained that the K_{SV} value of $Cr_2O_7^{2-}$ of **1** was calculated to be 3.1×10^4. The detection limits were 1.06×10^{-4}. In addition, the anti-interference ability of other inorganic

Table 1 Crystallographic data of complexes **1–2**

Complexes	1	2
Empirical formula	$C_{34}H_{36}N_4NiO_{11}S_2$	$C_{34}H_{36}N_4NiO_{11}S_2$
Fw	799.48	799.48
Crystal system	Monoclinic	Monoclinic
Space group	$C2/c$	$C2/c$
a (Å)	26.9946(15)	26.918(3)
b (Å)	9.3805(4)	9.3699(10)
c (Å)	16.4264(11)	16.2811(16)
β (°)	119.804(2)	119.653(2)
V (Å^3)	3609.4(4)	3568.6(7)
Z	4	4
T(K)	296(2)	273(2)
D_{calc} (g/cm^3)	1.471	1.488
μ/mm^{-1}	0.719	0.727
$F(000)$	1664.0	1664.0
R_{int}	0.0263	0.0571
R_1^a [$I > 2\sigma(I)$]	0.0330	0.0505
wR_2^b(all data)	0.0964	0.1443
GOF	1.003	1.048
$\Delta\rho_{max}$(e·Å^{-3})	0.350	0.582
$\Delta\rho_{min}$(e·Å^{-3})	− 0.237	− 0.497

^{a} $R_1 = \Sigma||F_o|–|F_c||/\Sigma|F_o|$, ^{b} $wR_2 = \Sigma[w(F_o^2–F_c^2)^2]/\Sigma[w(F_o^2)^2]^{1/2}$

Table 2 Sensing properties of **1** and **2**

Analytes		1	2
K_{SV} (M^{-1})	Fe^{3+}	2.8×10^4	1.7×10^4
	$Cr_2O_7^{2-}$	3.1×10^4	1.7×10^4
LOD	Fe^{3+}	1.18×10^{-4}	2.06×10^{-4}
	$Cr_2O_7^{2-}$	1.06×10^{-4}	2.06×10^{-4}

anions to $Cr_2O_7^{2-}$ anion by **1** was also explored. From Fig. 6d, it can be found that the peak intensity dropped sharply when $Cr_2O_7^{2-}$ was introduced into the prepared aqueous solution of 1 of different anions (Cl$^-$, Br$^-$, I$^-$, CH$_3$COO$^-$, CO$_3^{2-}$, HCO$_3^-$, NO$_3^-$, OH$^-$, and SO$_4^{2-}$), so the quenching effects of other anions on $Cr_2O_7^{2-}$ were hardly affected, which showed that 1 had good anti-interference to $Cr_2O_7^{2-}$ in aqueous solution. Polymer 2 shows the same effect (Fig. S7b–d and Table 2).

Conclusions

In summary, two 1D CPs with crossed-stacking modes were successfully constructed under hydrothermal conditions. The title CPs exhibited good electrochemical sensing activities for ascorbic acid, chloramphenicol, and KNO$_2$, which provided the possibility to become potential electrochemical sensing material. The $1-2$-CPEs can act as AA amperometric sensors. Furthermore, $1-2$ had similar multifunctional luminescence sensing properties to metal cations (Fe^{3+}) and inorganic anions ($Cr_2O_7^{2-}$). In short, the title CPs can be used as multifunctional electrochemical and fluorescent sensors to detect different pollutants. This work not only broadens the scope of application of CPs but also has greater significance in the field of environmental monitoring and protection. In addition, more CP-based multifunctional chemical sensors to determine environmentally harmful pollutants are further studied and explored.
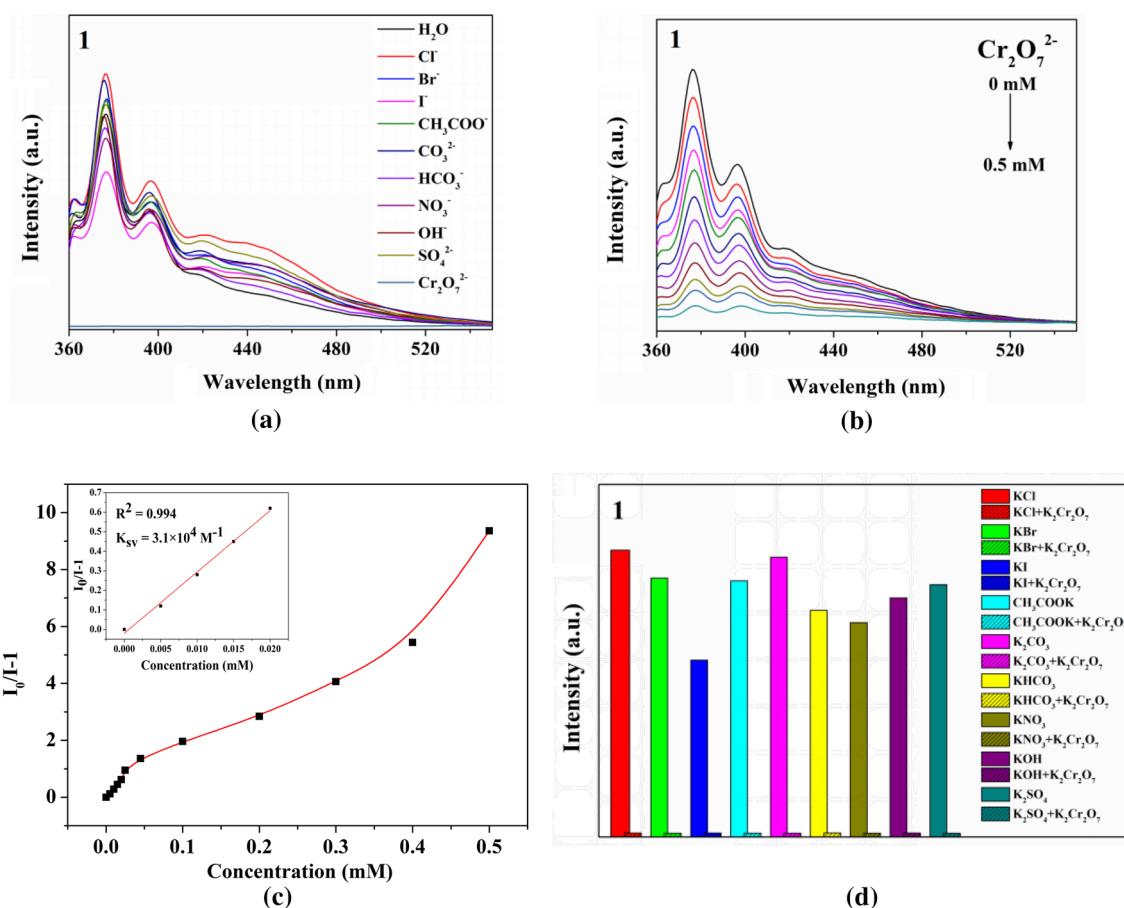
(a)

(b)

(c)

(d)

Fig. 6 **a** Fluorescence emission peak intensity of **1** in different anion solutions at the same excitation wavelength. **b** $Cr_2O_7^{2-}$ (10^{-3} M) concentration gradient experiment. **c** Linear relationship plot between fluorescence intensity and $Cr_2O_7^{2-}$ anions concentration. **d** Comparison of the luminescence emission peak intensity of 1 upon the addition of $Cr_2O_7^{2-}$

Declarations

Conflict of interest The authors declare that they have no conflict of interest.

References

1. Ma DY, Zhang SY, Zhan SH, Feng LT (2019) Ind Eng Chem Res 58:20090
2. Richardson JR, Fitsanakis V, Westerink RHS, Kanthasamy AG (2019) Acta Neuropathol 138:343–362
3. Feng DD, Zhao YD, Wang XQ, Fang DD (2019) Dalton Trans 48:10892–10900
4. Yu XP, Yang C, Song P, Peng J (2020) Tungsten 2:194–202
5. Bolisetty S, Peydayesh M, Mezzenga R (2019) Chem Soc Rev 48:463–487
6. Tian AX, Tian Y, Ning YL, Hou X (2016) Dalton Trans 45:13925–13936
7. Zhang J, Peh SB, Wang J, Du YH (2019) Chem Commun 55:4727–4730
8. Fu HR, Zhao Y, Xie T, Han ML (2018) J Mater Chem 6:6440
9. Tajik S, Beitollahi H, Nejad FG, Dourandish Z (2021) Ind Eng Chem Res 60:1112–1136
10. Bieber VS, Ozcelik E, Cox HJ, Ottley CJ (2020) ACS Appl Mater Interfaces 12:52136–52145
11. Sandford RC, Exenberger A, Worsfold PJ (2007) Environ Sci Technol 41:8420–8425
12. Shang XN, Kang HH, Chen YQ, Abdumutallip M (2021) Environ Sci Technol 55:9794–9804
13. Cabello NF, González PR, Castillo Á, Malherbe J (2012) Environ Sci Technol 46:12542–12549
14. Shakya R, Navarre DA (2006) J Agric Food Chem 54:5253–5260
15. Frenich AG, Torres MEH, Vega AB, Vidal JLM (2005) J Agric Food Chem 53:7371–7376
16. Hamilton EM, Young SD, Bailey EH, Humphrey OS (2021) Environ Sci Technol 55:2422–2429

17. Yang SL, Liu WS, Li G, Bu R (2020) Inorg Chem 59:15421–15429
18. Cui JW, Hou SX, Li YH, Cui GH (2017) Dalton Trans 46:16911–16924
19. Wu Y, Gu ZJ, Luo W, Wu L (2018) Transition Met Chem 43:673–681
20. Chen C, Xiong DK, Gu ML, Lu CX (2020) ACS Appl Mater Interfaces 12:35365–35374
21. Chai HM, Zhang GQ, Jiao CX, Ren YX (2020) ACS Omega 5:33039–33046
22. JindalS, Maka VK, Moorthy JN (2020) J Mater Chem C 8:11449−11456
23. Wu XQ, Feng PQ, Guo ZQ, Wei XH (2020) Langmuir 36:14123−14129
24. Song YP, Duan FH, Zhang S, Tian JY (2017) J Mater Chem A 5:19378–19389
25. Sheta SM, El-Sheikh SM, Osman DI, Salem AM (2020) Dalton Trans 49:8918–8926
26. Saraf M, Rajakb R, Mobin SM (2016) J Mater Chem A 4:16432–16445
27. Wang XY, Zhang J, Wei YA, Xing TY (2020) Analyst 145:1933–1942
28. Nagarkar SS, Desai AV, Samanta P, Ghosh SK (2015) Dalton Trans 44:15175–15180
29. Bhowal S, Ghosh A (2021) RSC Adv 11:27787–27800
30. Tian AX, Yang ML, Fu YB, Ying J (2019) Inorg Chem 58:4190–4200
31. Wang C, Ying J, Mou HC, Tian AX (2020) Inorg Chem Front 7:3882–3894
32. Yazigi FJ, Wilson C, Long DL, Forgan RS (2017) Cryst Growth Des 17:4739–4748
33. Jürgens E, Back O, Mayer JJ, Heinze K (2016) Z Naturforsch 71:1011–1018
34. Gurudevaru C, Gopalakrishnan M, Senthilkumar K, Hemachandran H (2018) Applied Organometallic Chem 32:3998
35. Subudhi S, Mansingh S, Swain G, Behera A (2019) Inorg Chem 58:4921–4934
36. Xu MZ, Li Q, Lv YY, Yuan ZM (2020) Tungsten 2:203–213
37. Buschbaum KM, Beuerle F, Feldmann C (2015) Micropor Mesopor Mat 216:171–199
38. Xue Z, Jia L, Zhu RR, Du L (2020) J Electroanal Chem 858:113783
39. Wang XL, Hu HL, Liu GC, Lin HY (2010) Chem Commun 46:6485–6487
40. Zhou Y, Hu Q, Yu F, Ran GY (2020) J Am Chem Soc 142:20313–20317
41. Du HJ, Wang CH, Li Y, Niu YY (2015) RSC Adv 5:74065–74074
42. Tian AX, Ni HP, Ji XB, Tian Y (2017) RSC Adv 7:5774–5781
43. Wang XL, Xiong Y, Liu GC, Lin HY (2018) Dalton Trans 47:9903–9911
44. Zheng YP, Tan Y, Zhou WL, Hao XR (2021) Inorg Chem 60:12323–12330
45. Argoubi W, Rabti A, Aoun SB, Raouafi N (2019) RSC Adv 9:37384–37390
46. Su CH, Sun CL, Liao YC (2017) ACS Omega 2:4245–4252
47. Lin HY, Wang XL, Hu HL, Chen BK (2009) Solid State Sci 11:643–650
48. Liu GC, Chen YQ, Wang XL, Chen BK (2009) J Solid State Chem 182:566–573
49. Huang QY, Tang WP, Yang Y, Liu W (2014) Z Naturforsch 69b:423–431
50. Wang KM, Du L, Ma YL, Zhao QH (2016) Transition Met Chem 41:573–580
51. Gao LL, Zhao QN, Li MM, Fan LM (2017) CrystEngComm 19:6651–6659
52. Xia YP, Li YW, Li DC, Yao QX (2015) CrystEngComm 17:2459–2463
53. Xiao Y, Li B, You ZX, Xing YH (2021) J Mater Chem C 9:3193–3203